Research Article | Vol. 25, No. 17 | 21 Aug 2017 | OPTICS EXPRESS 20780
Optics EXPRESS

Dual tunable plasmon-induced transparency based on silicon–air grating coupled graphene structure in terahertz metamaterial

HUI XU, HONGJIAN LI,* ZHIHUI HE, ZHIQUAN CHEN, MINGFEI ZHENG, AND MINGZHUO ZHAO

School of Physics and Electronics, Central South University, Changsha 410083, China
*lihj398@126.com

Abstract: A graphene plasmonic structure consists of three graphene layers mingled with a silicon–air grating is proposed. We theoretically predict and numerically simulate the plasmon-induced transparency effect in this system at terahertz wavelengths, and a dual plasmon-induced transparency peaks can be successfully tuned by virtually shifting the desired Fermi energy on graphene layers. We investigate the surface plasmon dispersion relation by means of analytic calculations, and we can achieve the numerical solution of propagation constant got by the dispersion relation. A suitable theoretical model is established to study spectral features in the plasmonic graphene system, and the theoretical results agree well with the simulations. The proposed model and findings may provide guidance for fundamental research of highly tunable optoelectronic devices.

OCIS codes: (240.6680) Surface plasmons; (160.3918) Metamaterials; (280.4788) Optical sensing and sensors.

References and links

1. Z. Bai and G. Huang, "Plasmon dromions in a metamaterial via plasmon-induced transparency," Phys. Rev. A **93**(1), 013818 (2016).
2. S. E. Harris, "Electromagnetically Induced Transparency," Phys. Today **50**(7), 36–42 (1997).
3. C. Sun, J. Si, Z. Dong, and X. Deng, "Tunable multispectral plasmon induced transparency based on graphene metamaterials," Opt. Express **24**(11), 11466–11474 (2016).
4. T. W. Ebbesen, C. Genet, and S. I. Bozhevolnyi, "Surface-plasmon circuitry," Phys. Today **61**(5), 44–50 (2008).
5. E. N. Economou, "Surface Plasmons in Thin Films," Phys. Rev. **182**(2), 539–554 (1969).
6. Z. He, H. Li, B. Li, Z. Chen, H. Xu, and M. Zheng, "Theoretical analysis of ultrahigh figure of merit sensing in plasmonic waveguides with a multimode stub," Opt. Lett. **41**(22), 5206–5209 (2016).
7. X. Zhao, L. Zhu, C. Yuan, and J. Yao, "Tunable plasmon-induced transparency in a grating-coupled double-layer graphene hybrid system at far-infrared frequencies," Opt. Lett. **41**(23), 5470–5473 (2016).
8. H. Wang, J. Yang, J. Zhang, J. Huang, W. Wu, D. Chen, and G. Xiao, "Tunable band-stop plasmonic waveguide filter with symmetrical multiple-teeth-shaped structure," Opt. Lett. **41**(6), 1233–1236 (2016).
9. Y. Huang, C. Min, P. Dastmalchi, and G. Veronis, "Slow-light enhanced subwavelength plasmonic waveguide refractive index sensors," Opt. Express **23**(11), 14922–14936 (2015).
10. A. K. Geim and K. S. Novoselov, "The rise of graphene," Nat. Mater. **6**(3), 183–191 (2007).
11. L. Ju, B. Geng, J. Horng, C. Girit, M. Martin, Z. Hao, H. A. Bechtel, X. Liang, A. Zettl, Y. R. Shen, and F. Wang, "Graphene plasmonics for tunable terahertz metamaterials," Nat. Nanotechnol. **6**(10), 630–634 (2011).
12. P.-Y. Chen, C. Argyropoulos, M. Farhat, and J. S. Gomez-Diaz, "Flatland plasmonics and nanophotonics based on graphene and beyond," Nanophotonics (2017).
13. Z. Sun, A. Martinez, and F. Wang, "Optical modulators with 2D layered materials," Nat. Photonics **10**(4), 227–238 (2016).
14. T. J. Echtermeyer, S. Milana, U. Sassi, A. Eiden, M. Wu, E. Lidorikis, and A. C. Ferrari, "Surface Plasmon Polariton Graphene Photodetectors," Nano Lett. **16**(1), 8–20 (2016).
15. C. Caucheteur, T. Guo, F. Liu, B. O. Guan, and J. Albert, "Ultrasensitive plasmonic sensing in air using optical fibre spectral combs," Nat. Commun. **7**, 13371 (2016).
16. S. X. Xia, X. Zhai, L. L. Wang, B. Sun, J. Q. Liu, and S. C. Wen, "Dynamically tunable plasmonically induced transparency in sinusoidally curved and planar graphene layers," Opt. Express **24**(16), 17886–17899 (2016).
17. L. A. Ponomarenko, A. K. Geim, A. A. Zhukov, R. Jalil, S. V. Morozov, K. S. Novoselov, I. V. Grigorieva, E. H. Hill, V. V. Cheianov, V. I. Fal'ko, K. Watanabe, T. Taniguchi, and R. V. Gorbachev, "Tunable metal–insulator transition in double-layer graphene heterostructures," Nat. Phys. **7**(12), 958–961 (2011).
18. P. Zhang, N.-H. Shen, T. Koschny, and C. M. Soukoulis, "Surface-Plasmon-Mediated Gradient Force Enhancement and Mechanical State Transitions of Graphene Sheets," ACS Photonics **4**(1), 181–187 (2017).

#303067 https://doi.org/10.1364/OE.25.020780
Journal © 2017 Received 24 Jul 2017; revised 11 Aug 2017; accepted 11 Aug 2017; published 17 Aug 2017

Optics EXPRESS

19. A. Y. Zhu, A. I. Kuznetsov, B. Luk'yanchuk, N. Engheta, and P. Genevet, "Traditional and emerging materials for optical metasurfaces," Nanophotonics **6**(2), 452–471 (2017).
20. P. Qiu, W. Qiu, Z. Lin, H. Chen, J. Ren, J. X. Wang, Q. Kan, and J. Q. Pan, "Dynamically Tunable Plasmon-Induced Transparency in On-chip Graphene-Based Asymmetrical Nanocavity-Coupled Waveguide System," Nanoscale Res. Lett. **12**(1), 374 (2017).
21. C. Sun, Z. Dong, J. Si, and X. Deng, "Independently tunable dual-band plasmonically induced transparency based on hybrid metal-graphene metamaterials at mid-infrared frequencies," Opt. Express **25**(2), 1242–1250 (2017).
22. K. S. Yee, "Numerical solution of initial boundary value problems involving maxwell's equations in isotropic media," IEEE Trans. Antenn. Propag. **14**(3), 302–307 (1966).
23. C. H. Gan, H. S. Chu, and E. P. Li, "Synthesis of highly confined surface plasmon modes with doped graphene sheets in the midinfrared and terahertz frequencies," Phys. Rev. B **85**(12), 125431 (2012).
24. A. N. Grigorenko, M. Polini, and K. S. Novoselov, "Graphene plasmonics," Nat. Photonics **6**(11), 749–758 (2012).
25. A. Vakil and N. Engheta, "Transformation optics using graphene," Science **332**(6035), 1291–1294 (2011).
26. M. Jablan, H. Buljan, and M. Soljačić, "Plasmonics in graphene at infrared frequencies," Phys. Rev. B **80**(24), 245435 (2009).
27. K. L. Tsakmakidis, L. Shen, S. A. Schulz, X. Zheng, J. Upham, X. Deng, H. Altug, A. F. Vakakis, and R. W. Boyd, "Breaking Lorentz reciprocity to overcome the time-bandwidth limit in physics and engineering," Science **356**(6344), 1260–1264 (2017).
28. H. A. Haus and W. Huang, "Coupled-Mode Theory," Proc. IEEE **79**, 1505–1518 (1991).
29. H. Xu, H. Li, B. Li, Z. He, Z. Chen, and M. Zheng, "Influential and theoretical analysis of nano-defect in the stub resonator," Sci. Rep. **6**(1), 30877 (2016).
30. S. Balci, O. Balci, N. Kakenov, F. B. Atar, and C. Kocabas, "Dynamic tuning of plasmon resonance in the visible using graphene," Opt. Lett. **41**(6), 1241–1244 (2016).
31. Z. Fei, A. S. Rodin, G. O. Andreev, W. Bao, A. S. McLeod, M. Wagner, L. M. Zhang, Z. Zhao, M. Thiemens, G. Dominguez, M. M. Fogler, A. H. Castro Neto, C. N. Lau, F. Keilmann, and D. N. Basov, "Gate-tuning of graphene plasmons revealed by infrared nano-imaging," Nature **487**(7405), 82–85 (2012).

1. Introduction

Plasmon-induced transparency (PIT) is a typical destructive interference effect resulting from the strong coupling between two excitation states in meta-atoms of metamaterials, and it is a kind of analogues of electromagnetically induced transparency (EIT) [1, 2]. In general, the PIT effect can remarkably slow down photons velocities and enhance nonlinear properties [3]. Besides, surface plasmon polaritons (SPPs) which are polariton modes of photon and electron density waves along a conductor and dielectric interface have undisputed advantages like strong enhancement of the local electric field and much better adaptability to nano architectures [4, 5]. So of course it has many underlying practical applications. For example, a large number of applications in optical sensors [6], optical switch [7], plasmonic waveguide filters [8] and slow light effect [9] have been proposed up to now. The PIT effect can be realized in the proposed applications, but PIT peaks are all modulated only by carefully changing geometric parameters of structures.

Graphene, a two-dimensional (2D) material composed of single-layer carbon atom in a honeycomb lattice, has attracted much attention in the past decade because it exhibits almost all the electrical properties and functions required for integrated photonic circuits [10, 11]. Considering its unique properties and highly reactive electric response, graphene can also support propagation of SPPs and it results in strongly localized plasmons residing within from near-infrared to terahertz region. In contrast to noble metals, graphene plasmonic resonances can be dynamically tuned through electrostatic biasing and enable a new generation of reconfigurable plasmonic devices. Therefore, it is proved as a promising material for multifarious plasmonic systems due to its remarkable characteristics, such as strong mode confinement, low loss, and active tunability. Compared with traditional bulk semiconductors, 2D graphene materials also provide additional values, such as mechanical flexibility, easy fabrication and integration. With those advantages, graphene provides a great opportunity in many plasmonic devices, such as modulators [12, 13], photodetectors [14], sensors [15] and many other practical applications [16–19].

In our paper, a novel graphene based on silicon–air grating structure is proposed to realize PIT phenomenon. We can achieve a dual-PIT peak by changing Fermi energy of the graphene

Optics EXPRESS

layers at infrared and terahertz (THz) wavelengths in the designed structure. In contrast to the metal plasmonic waveguide structure [20], our graphene system has competitive advantages that the PIT can be tuned by extra gate voltage not geometric parameters. Furthermore, compared with the patterned or separating graphene devices [21], the graphene in our structure keeps continuous form. It has the benefit of preserving the high mobility of graphene and also simplifies these fabrication processes. Moreover, the modulation of PIT peaks with three graphene layers is investigated in detail. The designed structure exhibits a prominent PIT resonance peak in the finite-difference time-domain (FDTD) [22] simulated transmission spectrum, and its resonance mechanism is further discussed by the coupled mode theory (CMT). Furthermore, numerical simulation results for the PIT effects show a good agreement with theoretical expectations. Thus it can be achieved for building high performance active plasmonic devices, and the presented theoretical model and the pronounced features of this simple graphene plasmonic structure, such as the tunable PIT phenomenon and convenient integration, may have potential applications in the sensors, tunable switches, and slow light devices.

2. Structure and theoretical model

The schematic of dual-PIT graphene device, which is composed of three graphene layers separated with the dielectric silicon and air by a grating shape, is illustrated in Fig. 1(a). Most structural information of the system is also introduced in Fig. 1. The three graphene layers are separated by a dielectric spacer of thickness d_1 and d_2, respectively.

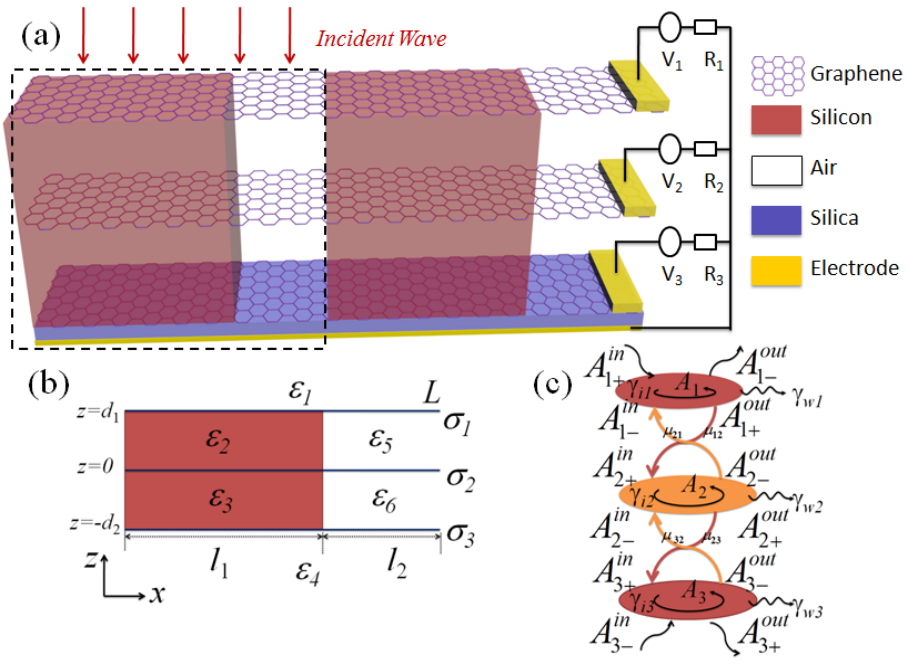

Fig. 1. (a) Schematic illustration of the three layers graphene structure. The red dielectric is silicon, the blue is a silica substrate, the yellows are the electrode and the other dielectrics are air. (b) A front view of Fig. 1(a) which is a period surrounded by the black frame (The period L = 400nm, d_1 = 250nm, d_2 = 250nm, l_1 = 250nm, and l_2 = 150nm). (c) An equivalent theoretical coupled model for this graphene-based plasmonic resonators.

Numerical simulation method in this letter is selected as the finite-difference time-domain (FDTD). For simplicity, the spacer is assumed to be air with a permittivity of 1.00 in the simulation. A TM-polarized wave is injected along the negative direction of z-axis. For the sake of the clarity of presentation, the Kubo formula has governed the surface conductivity of

Optics EXPRESS

graphene including the intraband and interband transition contributions, and then the conductivity of graphene σ obtains a Drude-like expression [23], as follows:

$$\sigma = \frac{ie^2 E_F}{\pi\hbar^2(\omega + i\tau^{-1})} \tag{1}$$

here, this equation is built based on assumption $(E_F, \hbar\omega) \gg k_B T$ when temperature $T = 300$K in the near-infrared to THz region. The parameters are explained as follows, e is the elementary charge, E_F is the Fermi energy, k_B is the Boltzmann constant, $\hbar$ is the reduced Planck constant, ω is the angular frequency, and τ is the carrier relaxation time which satisfies the relationship $\tau = \mu E_F / (ev_F^2)$ (where $\mu = 3.00$ m^2/ (V·s) is the measured DC mobility, $v_F = 10^6$ m/s is the Fermi velocity [10, 24]). The simulations are performed with the two-dimensional FDTD method with mesh grid size $\Delta x = 1$ nm and $\Delta z = 0.1$nm, respectively. The y-axis can be regarded as infinite. The calculated domain is surrounded by perfectly matched layer absorbing boundary at z-directions and periodic boundary at x-directions, respectively.

Now, we present the derivation of the relationship between thickness and wave vector of electromagnetic mode guided by graphene. TM wave is characterized by the existence of a H_y component of the magnetic field together with E_x and E_z components of the electric field. Here, x is the direction of propagation, z is the direction normal to the graphene, and y is the direction parallel to the graphene and perpendicular to z. The structure is surrounded with dielectrics of constants $\varepsilon_1 = 1.0$ (air, on top of structure) and $\varepsilon_4 = 3.9$ (silica, the substrate of structure). For definiteness we use $\varepsilon_5 = \varepsilon_6 = 1.0$ for air dielectric grating, and $\varepsilon_2 = \varepsilon_3 = 11.9$ corresponding to silicon dielectric grating, which corresponds to a typical experimental setup [24]. According to Maxwell equations of $\nabla\times\vec{H} = -i\omega\varepsilon_0\varepsilon_d\vec{E}$, $\nabla\times\vec{E} = i\omega\mu_0\mu_d\vec{H}$ and the component of the wave vector perpendicular to the interface in the three layer graphene $k_i \equiv k_{z,i}$ $(i = 1, 2, 3)$, the expression of electric and magnetic fields is given as follows:

$$\begin{aligned} &Region\,1\,(z > d_1):\\ &H_{y1} = Ae^{i\beta x}e^{-k_1 z} \end{aligned} \tag{2}$$

$$E_{x1} = iA\frac{k_1}{\omega\varepsilon_0\varepsilon_1}e^{i\beta x}e^{-k_1 z} \tag{3}$$

$$E_{z1} = -A\frac{\beta}{\omega\varepsilon_0\varepsilon_1}e^{i\beta x}e^{-k_1 z} \tag{4}$$

$$\begin{aligned} &Region\,2\,(0 < z < d_1):\\ &H_{y2} = Be^{i\beta x}e^{k_2 z} + Ce^{i\beta x}e^{-k_2 z} \end{aligned} \tag{5}$$

$$E_{x2} = -iB\frac{k_2}{\omega\varepsilon_0\varepsilon_2}e^{i\beta x}e^{k_2 z} + iC\frac{k_2}{\omega\varepsilon_0\varepsilon_2}e^{i\beta x}e^{-k_2 z} \tag{6}$$

$$E_{z2} = -B\frac{\beta}{\omega\varepsilon_0\varepsilon_2}e^{i\beta x}e^{-k_2 z} - C\frac{\beta}{\omega\varepsilon_0\varepsilon_2}e^{i\beta x}e^{-k_2 z} \tag{7}$$

$$H_{y3} = De^{i\beta x}e^{k_3 z} + Ee^{i\beta x}e^{-k_3 z} \tag{8}$$

$$E_{x3} = -iD\frac{k_3}{\omega\varepsilon_0\varepsilon_3}e^{i\beta x}e^{k_3 z} + iE\frac{k_3}{\omega\varepsilon_0\varepsilon_3}e^{i\beta x}e^{-k_3 z} \tag{9}$$

Optics EXPRESS

$$E_{z3} = -D\frac{\beta}{\omega\varepsilon_0\varepsilon_3}e^{i\beta x}e^{-k_3 z} - E\frac{\beta}{\omega\varepsilon_0\varepsilon_3}e^{i\beta x}e^{-k_3 z} \tag{10}$$

$$\begin{aligned} &Region\ 4\,(z < -d_2):\\ &H_{y4} = Fe^{i\beta x}e^{k_4 z} \end{aligned} \tag{11}$$

$$E_{x4} = -iF\frac{k_4}{\omega\varepsilon_0\varepsilon_4}e^{i\beta x}e^{k_4 z} \tag{12}$$

$$E_{z4} = -F\frac{\beta}{\omega\varepsilon_0\varepsilon_4}e^{i\beta x}e^{k_4 z} \tag{13}$$

Finally, with the combination of the above equations, continuity of the tangential electric field($E_{x1} = E_{x2}$), boundary condition for the tangential magnetic field(H_2-$H_1 = \sigma E_x$) [25, 26], $k_1^2 = \beta^2 - \varepsilon_1 k_0^2$, $k_4^2 = \beta^2 - \varepsilon_4 k_0^2$ and $k_2^2 = k_3^2 = \beta^2 - \varepsilon_2 k_0^2$ (β is propagation constant and k_0 is the wave vector of the propagating wave in free space, respectively), the dispersion relation for the TM SPP is implicitly given as

$$\frac{(\frac{\varepsilon_2}{k_2}+\frac{\varepsilon_4}{k_1}+\frac{i\sigma}{\omega\varepsilon_0})e^{2k_2 d_1}}{-\frac{\varepsilon_2}{k_2}+\frac{\varepsilon_4}{k_1}+\frac{i\sigma}{\omega\varepsilon_0}} = \frac{(\frac{\varepsilon_2}{k_2}+\frac{\varepsilon_2}{k_2}-\frac{i\sigma}{\omega\varepsilon_0})(-\frac{\varepsilon_2}{k_2}+\frac{\varepsilon_1}{k_1}+\frac{i\sigma}{\omega\varepsilon_0})+\frac{i\sigma}{\omega\varepsilon_0}(\frac{\varepsilon_2}{k_2}+\frac{\varepsilon_1}{k_1}+\frac{i\sigma}{\omega\varepsilon_0})e^{2k_2 d_1}}{-\frac{i\sigma}{\omega\varepsilon_0}(-\frac{\varepsilon_2}{k_2}+\frac{\varepsilon_1}{k_1}+\frac{i\sigma}{\omega\varepsilon_0})+(\frac{\varepsilon_2}{k_2}+\frac{\varepsilon_2}{k_2}+\frac{i\sigma}{\omega\varepsilon_0})(\frac{\varepsilon_2}{k_2}+\frac{\varepsilon_1}{k_1}+\frac{i\sigma}{\omega\varepsilon_0})e^{2k_2 d_1}} \tag{14}$$

From this equation, the propagation constant β of the graphene SPPs can be obtained. As a result, we can readily get the effective mode index of SPP, defined as $n_{eff} = \beta/k_0$. As a proof of this concept, the real part of propagation constant β and effective index n_{eff} are numerically plotted in the Fig. 2(a) and 2(b), respectively. Obviously, from the Fig. 2(b), Re(n_{eff}) decreases for a fixed wavelength as the Fermi energy E_F increases, which intends the graphene SPPs are better confined at lower Fermi energy. Importantly, with a slight change in Fermi energy, the Re(n_{eff}) varies greatly, which leads to the design of dynamically tunable peak modulation devices.

Optics EXPRESS

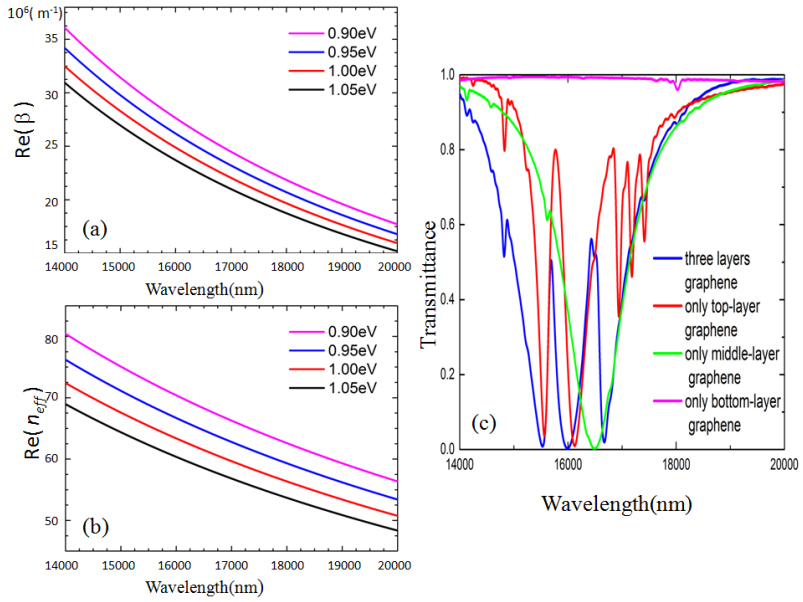

Fig. 2. (a) The dispersion relation of this TM SPP surface wave with different Fermi energy. (b) The real parts of effective refractive index of the plasmonic mode at the three layers graphene structure with different Fermi energy. (c) Transmission spectra of the hybrid system with three layers graphene (bule), only top-layer graphene (red), only middle-layer graphene (green), and only bottom-layer graphene (purple) as Fermi energy E_F = 1.0eV.

As frequency increases into the far-infrared, the surface wave becomes more tightly confined to the graphene layer, but becomes slow as energy is concentrated on the graphene surface. In this three layers graphene system, Fig. 2(c) shows the transmission spectra of the hybrid system with three layers graphene (blue), only upper-layer graphene (red), only middle-layer graphene (green), and only lower-layer graphene (purple) as Fermi energy E_F = 1.0eV. From the spectra, we can see that the top layer graphene at $z = d_1$ and the middle layer graphene at $z = 0$ couple efficiently to the incident wave, thus, the graphene SPPs are strongly excited which act as two excitation states and two wide continuum spectra are formed. However, the bottom layers graphene at $z = -d_2$ couples weakly to the incident wave and leads to a narrow discrete one which play another excitation state. In other words, the top and middle layers graphene act as two bright elements, and the bottom layer graphene act as a dark elements. Therefore, a dual-PIT resonance results from the destructive interference between the bright and dark plasmon elements as showed in Fig. 2(c) and Fig. 3. More specific analysis to the activated modes will be described in detail at in later content.

With the incident waves pass through z-direction, the energy can be coupled into the three layers graphene and the dynamic transmittance characteristics of our proposed structure can be investigated by the CMT [27–29]. As shown in Fig. 1(c), the three equivalent resonators are named as A_1, A_2 and A_3 take the place of the excitation state modes, respectively. The incoming and outgoing waves in the resonators are depicted by $A_{n\pm}^{in}$ and $A_{n\pm}^{out}$ (n = 1, 2, 3). The subscript ± represent two propagating directions of waveguide modes, as shown in Fig. 1(c). Thus, the complex amplitude a_n of the nth resonator (n = 1, 2, 3) can be expressed as

Optics EXPRESS

$$\begin{pmatrix} \gamma_1 & -i\mu_{12} & -i\mu_{13} \\ -i\mu_{21} & \gamma_2 & -i\mu_{23} \\ -i\mu_{31} & -i\mu_{32} & \gamma_3 \end{pmatrix} \cdot \begin{pmatrix} a_1 \\ a_2 \\ a_3 \end{pmatrix} = \begin{pmatrix} \sqrt{\frac{1}{\tau_{w1}}} & 0 & 0 \\ 0 & \sqrt{\frac{1}{\tau_{w2}}} & 0 \\ 0 & 0 & \sqrt{\frac{1}{\tau_{w3}}} \end{pmatrix} \cdot \begin{pmatrix} A_{1+}^{in} + A_{1-}^{in} \\ A_{2+}^{in} + A_{2-}^{in} \\ A_{3+}^{in} + A_{3-}^{in} \end{pmatrix} \tag{15}$$

here, $\gamma_n = \left(i\omega - i\omega_n - \frac{1}{\tau_{in}} - \frac{1}{\tau_{wn}} \right)$ (n = 1, 2, 3), ω is the angular frequency of the incident waves, ω_n (n = 1, 2, 3) is the nth resonant angular frequency, $\gamma_{in} = 1/\tau_{in}$ is the decay rate due to intrinsic loss, $\gamma_{wn} = 1/\tau_{wn}$ is the decay rate due to energy escaping into outside space from the resonant(n = 1, 2, 3), and μ_{nm} is the coupling coefficient between is the coupling coefficients between the nth and mth modes(n = 1, 2, 3, m = 1, 2, 3, $n \neq m$), respectively. Along the conservation of energy, they also satisfy the following relations

$$A_{n+}^{in} = A_{(n-1)+}^{out} e^{i\varphi_{n-1}}, A_{(n-1)-}^{in} = A_{n-}^{out} e^{i\varphi_{n-1}} (n = 2,3) \tag{16}$$

$$A_{n+}^{out} = A_{n+}^{in} - \sqrt{\frac{1}{\tau_{wn}}} a_n, A_{n-}^{out} = A_{n-}^{in} - \sqrt{\frac{1}{\tau_{wn}}} a_n (n = 1,2,3) \tag{17}$$

here, $\varphi_n = \mathrm{Re}(\beta) d_n$ (n = 1, 2) represents the phase shift (d_n is the coupling distance between nth and (n + 1)th resonant modes). In our proposed structure, $d_1 = d_2$, and so $\varphi_1 = \varphi_2$.

According to Eqs. (15)-(17) and the condition that the wave is only injected from the upper layer ($A_{3-}^{in} = 0$), we can achieve the complex transfer coefficient of this system

$$t = \frac{A_{3+}^{out}}{A_{1+}^{in}} = t_0 - \frac{b_1 t_1 - b_2 t_2}{b_3 \gamma_1} \tag{18}$$

where,

$$t_0 = e^{2i\varphi} + \frac{1}{\tau_{\omega 1} \gamma_1} e^{2i\varphi} \tag{19}$$

$$\begin{aligned} \mathrm{t}_1 = & \sqrt{\frac{1}{\tau_{\omega 3}}} \gamma_1 (\gamma_1 \gamma_2 - \chi_{12} \chi_{21}) + \sqrt{\frac{1}{\tau_{\omega 1}}} e^{2i\varphi} \chi_{12} (\chi_{13} \chi_{21} + \gamma_1 \chi_{23}) + \\ & \sqrt{\frac{1}{\tau_{\omega 1}}} e^{2i\varphi} (\gamma_1 \gamma_2 - \chi_{12} \chi_{21}) \chi_{13} + \sqrt{\frac{1}{\tau_{\omega 2}}} e^{i\varphi} \gamma_1 (\chi_{13} \chi_{21} + \gamma_1 \chi_{23}) \end{aligned} \tag{20}$$

$$\begin{aligned} t_2 = & \sqrt{\frac{1}{\tau_{\omega 3}}} \gamma_1 (\chi_{31} \gamma_2 + \chi_{21} \chi_{32}) + \sqrt{\frac{1}{\tau_{\omega 1}}} e^{2i\varphi} \chi_{12} (\chi_{31} \chi_{23} + \chi_{21} \gamma_3) + \\ & \sqrt{\frac{1}{\tau_{\omega 1}}} e^{2i\varphi} (\chi_{31} \gamma_2 + \chi_{21} \chi_{32}) \chi_{13} + \sqrt{\frac{1}{\tau_{\omega 2}}} e^{i\varphi} \gamma_1 (\chi_{31} \chi_{23} + \chi_{21} \gamma_3) \end{aligned} \tag{21}$$

$$b_1 = \chi_{31} e^{i\varphi} \sqrt{\frac{1}{\tau_{\omega 2}}} - \chi_{21} e^{2i\varphi} \sqrt{\frac{1}{\tau_{\omega 3}}} \tag{22}$$

Optics EXPRESS

$$b_2 = \gamma_1 e^{i\varphi}\sqrt{\frac{1}{\tau_{\omega 2}}} + \chi_{21}\sqrt{\frac{1}{\tau_{\omega 1}}} \tag{23}$$

$$b_3 = (\gamma_1\gamma_2 - \chi_{12}\chi_{21})(\chi_{31}\chi_{23} + \chi_{21}\gamma_3) - (\chi_{31}\gamma_2 + \chi_{21}\chi_{32})(\chi_{13}\chi_{21} + \gamma_1\chi_{23}) \tag{24}$$

$$\chi_{mn} = \sqrt{\frac{1}{\tau_{wm}\tau_{wn}}}e^{i\varphi} + i\mu_{mn}(m = 1,2,3; n = 1,2,3; m \neq n) \tag{25}$$

Thus, the transmittance can be obtained as $T = |t|^2$.

3. Simulation and discussion

Next, we study the optical characteristics of our proposed structure. By properly setting separation distance d, Fermi energy E_F and mobility μ of the three graphene layers, the resonance characteristics of plasmonic modes supported by the graphene could be accurately controlled. And then, a desired PIT effect can be obtained. The tuning scheme is outlined in Fig. 1(a) and is based on applying a voltage difference across the dielectric layer to inject or remove electrons from the graphene layers and modify their Fermi energy. Throughout this letter, the geometric parameters are fixed, like as L = 400nm, l_1 = 250nm, l_2 = 150nm, d_1 = 250nm and d_2 = 250nm. Based on the above analysis, we numerically calculated the transmission spectra of the grapheme plasmonic system with different Fermi energy E_F = 1.05eV, 1.00eV, 0.95eV, 0.90eV, respectively, and electrical tuning of the transparency window has a close relation with the Fermi energy level as shown in Fig. 3. The Fermi energy of graphene could be experimentally modified from 0.2eV to 1.2eV after applying a high bias voltage [30]. Thus in this system, we reasonably assume that Fermi energy E_F can be dynamically tuned from 0.90eV to 1.05eV. The decay rates and the coupling coefficients obtained from theoretical calculation and the FDTD simulations are fitting parameters and their values are showed in the caption of Fig. 3. Then we put these parameters into Eq. (18)-(25) and get theoretical transmission curves, which agree well with the simulation results. This consistence also reveals that the formation of plasmon induced transparency can be described as the coupling between cavities in our system. In Fig. 3, the blue solid lines are simulated transmittance and the red cycle lines are theoretical fitting, respectively. And we can see that the FDTD simulations are in excellent agreement with the theoretical fittings, from which we can conclude that Eq. (18) is a qualified theoretical description of plasmon-induced transparency in the plasmonic graphene system. So, the theoretical analysis allows us to understand the response of the plasmonic graphene system as a function of their microscopic parameters. As we can see from the blue lines, the transmission spectrum exhibits an obvious dual-PIT peak for each value of Fermi energy. In this stacked graph, we can clearly see that the resonant wavelength blue shift with Fermi energy E_F increases.

Optics EXPRESS

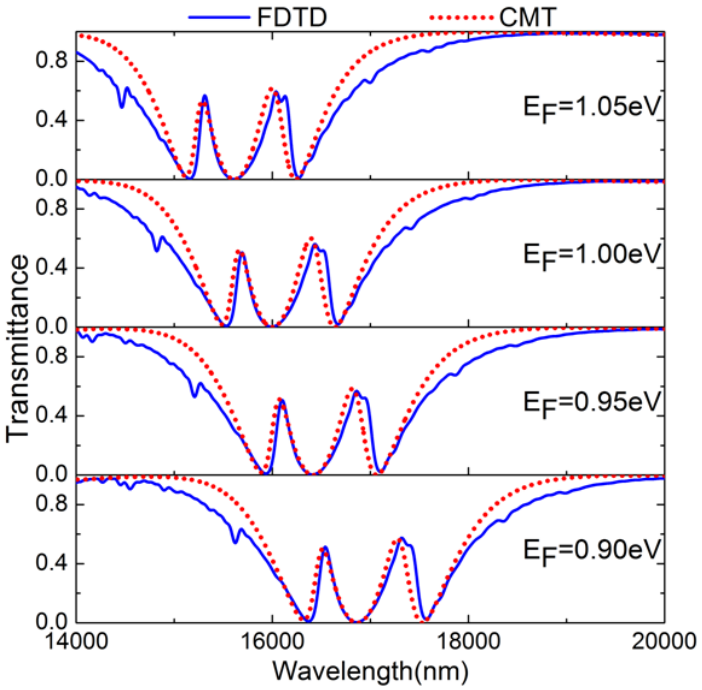

Fig. 3. The simulated transmittance (blue solid lines) and theoretical fitting (red cycle lines) as E_F = 1.05eV, 1.00eV, 0.95eV, 0.90eV in the three layers graphene structure, respectively. For theoretical transmission spectra and structural properties of graphene, the decay rates are γ_{w1} = 0.38 × 10^{12} rad/s, γ_{w2} = 3.15 × 10^{12} rad/s, γ_{w3} = 1.52 × 10^{12} rad/s, γ_{i1} = 2.55 × 10^{11} rad/s, γ_{i2} = 1.21 × 10^{11} rad/s, and γ_{i3} = 0.23 × 10^{11} rad/s, respectively. The coupling coefficients are μ_{12} = 6.38 × 10^{11} rad/s, μ_{21} = 6.38 × 10^{11} rad/s, μ_{13} = 2.27 × 10^{11} rad/s, μ_{31} = 2.27 × 10^{11} rad/s, μ_{23} = 6.38 × 10^{11} rad/s, and μ_{32} = 6.38 × 10^{11} rad/s, respectively.

To get more insight into the physical mechanism of this observed dual-PIT effects, Fig. 4 shows the peaks and dips of the spectral transmittance with Fermi energy E_F varying from 0.90eV to 1.05eV. To illustrate a difference, the dip at the shortest wavelength is called as dip1, the dip at the longest wavelength is called as dip3, and the middle one is called as dip2. The peak which lies between dip1 and dip2 is called as peak1 and which lies between dip2 and dip3 is called as peak2, respectively. We can see the approximately linear relationship of the peak/dip wavelengths versus the Fermi energy E_F. In order to elaborate this phenomenon, we have theoretically modeled the effects of dual-PIT on the Fermi energy E_F from 0.90eV to 1.05eV, as showed in Fig. 5(b).

FDTD simulated electric field intensities of THz metamaterial with three graphene layers are showed in the Figs. 4(c)-4(f) with Fermi energy E_F = 0.9eV at dip1, dip2, dip3 and E_F = 0.95eV at dip, dip2, dip3, respectively. Here, these field intensities provide a basic understanding of the mechanisms involved. From the field intensity diagrams, we can get that the SPPs mode is excited at the interface of graphene–silicon boundary. At transmission dip 1 and transmission dip2, only the top graphene layer is excited, and the other two layers are not excited. However, at dip3, the two upper layers are excited at the same time and the bottom layer is still not directly excited. Through above simulation and analysis, we can draw a conclusion that the two upper graphene layers can be regarded as two bright elements and the bottom graphene layer acts as a dark element. The two modes at lower wavelength are together excited by the top and bottom graphene layers and the mode at maximum wavelength is excited by the middle and bottom graphene layers, respectively. So, the three resonance modes are together controlled by the three graphene layers. The bottom graphene

Optics EXPRESS

layer cannot be excited by the incident wave functioning as the dark element, and the destructive interference between the bright and dark elements give rise to a dual-PIT effect.

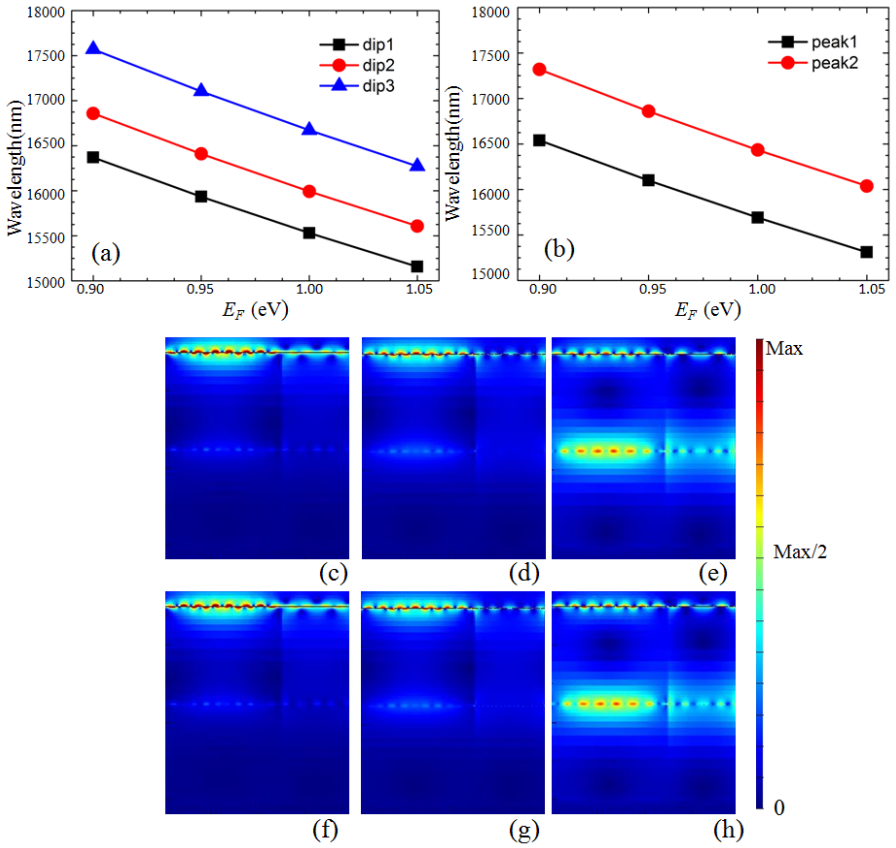

Fig. 4. (a) The wavelength values of dip as a function of Fermi energy E_F. (b) The wavelength values of peak as a function of Fermi energy E_F. (c)-(e) Simulated electric field intensities profile with the graphene Fermi energy E_F = 0.9eV at λ = 16369.9nm, 16858.6nm, 17569.4nm, respectively. (f)-(h) Simulated electric field intensities profile with the graphene Fermi energy E_F = 0.95eV at λ = 15934.1nm, 16410nm, 17102.7nm, respectively.

The dispersion characteristics of plasmonic modes in the three graphene layers device can be obtained by solving the Eq. (14). From the equations, we can see that the dispersion characteristics are dependent on the surface conductivity of graphene, which can be controlled by the Fermi energy. What is more, we can tune the Fermi energy by the applied bias voltage V_g [31], like following formula

$$E_F = \hbar v_F \sqrt{\frac{\pi \varepsilon_0 \varepsilon_d V_g}{d_{sub} e}} \tag{26}$$

where, d_{sub} is the thickness of insulated substrate material (silica). Using above formula, we can plot an evolution of the Fermi energy E_F versus bias voltage V_g, as showed in the Fig. 5(a). Because the graphene layers in our plasmonic system exist in a continuous whole block, it is much easier to structurally realize the tunability compared with other discrete graphene tunable devices. Furthermore, to investigate spectral characteristics more specifically, the evolution of the transmission spectra versus Fermi energy E_F and wavelength λ is displayed in Fig. 5(b). As expected, Fig. 5(b) shows that there are three transmission dips which present blue shift with the increase of Fermi energy. Moreover, the transparent resonance dips and

Optics EXPRESS

peaks exhibit a linear relationship. Figure 5(b) clearly shows that the resonance characteristics of the proposed graphene plasmonic system are efficiently tuned by altering the Fermi energy E_F from 0.90eV to 1.05eV.

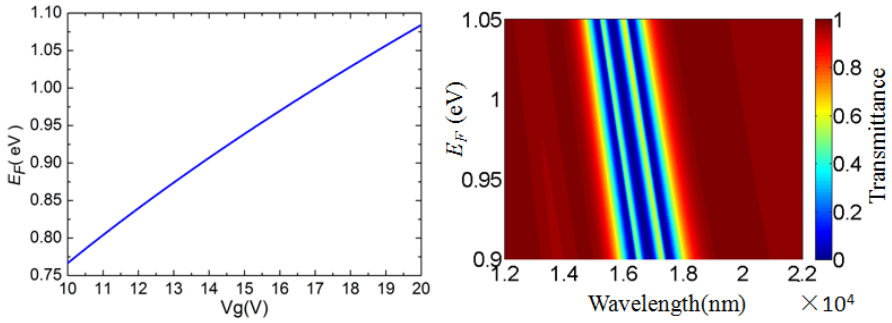

Fig. 5. (a) The Fermi energy E_F as a function of the applied bias voltage V_g (b) Evolution of the transmission spectra versus Fermi energy E_F and wavelength λ.

4. Conclusion

In summary, by using the temporal CMT and FDTD method, we have proposed and demonstrated a tunable dual-PIT phenomenon by means of three layers graphene nanostructures based on silicon–air grating structure, and the metamaterial is designed at terahertz frequencies. At first, we analyze the dispersion relations of our proposed structure. Re(β) and Re(n_{eff}) decrease for a fixed wavelength as the Fermi energy E_F increases. Then, the numerical results are calculated by FDTD method for different Fermi energy E_F and the theoretical results are calculated by CMT for different Fermi energy E_F. The consistency between the theoretical and numerical results validates the correctness of the theoretical description. Compared with the devices based on patterned and separating graphene, our structure keeps graphene in the continuous form. It has the benefit of preserving the high mobility of graphene and also simplifies the fabrication processes. With these advantages and the impressive dual-PIT resonance characteristics, our proposed graphene metamaterial structure may open up avenues for terahertz devices and sensing technology, and may provide meaningful guidance and potential applications for designing graphene metamaterials.

Funding

This work is supported by the Hunan Provincial Innovation Foundation for Postgraduate (Grant No. CX2017B042) and the National Natural Science Foundation of China (Grant No. 61275174).